Translational Oncology
www.transonc.com

Volume 9 Number 6 December 2016 pp. 521–530 521

A Comparative Performance Analysis of Multispectral and RGB Imaging on HER2 Status Evaluation for the Prediction of Breast Cancer Prognosis[1]

Wenlou Liu*, Linwei Wang*, Jiuyang Liu*, Jingping Yuan†, Jiamei Chen*, Han Wu*, Qingming Xiang*, Guifang Yang‡ and Yan Li*,§

*Department of Oncology, Zhongnan Hospital of Wuhan University, Hubei Key Laboratory of Tumor Biological Behaviors & Hubei Cancer Clinical Study Center, Wuhan, 430071, China; †Department of Pathology, Renmin Hospital of Wuhan University, Wuhan, 430060, China; ‡Department of Pathology, Zhongnan Hospital of Wuhan University, Wuhan, 430071, China; §Department of Peritoneal Cancer Surgery, Beijing Shijitan Hospital Affiliated to the Capital Medical University, Beijing, 100038, China

Abstract

Despite the extensive application of multispectral imaging (MSI) in biomedical multidisciplinary researches, there is a paucity of data available regarding the implication of MSI in tumor prognosis prediction. We compared the behaviors of multispectral (MS) and conventional red-green-blue (RGB) images on assessment of human epidermal growth factor receptor 2 (HER2) immunohistochemistry to explore their impact on outcome in patients with invasive breast cancer (BC). Tissue microarrays containing 240 BC patients were introduced to compare the performance of MS and RGB imaging methods on the quantitative assessment of HER2 status and the prognostic value of 5-year disease-free survival (5-DFS). Both the total and average signal optical density values of HER2 MS and RGB images were analyzed, and all patients were divided into two groups based on the different 5-DFS. The quantification of HER2 MS images was negatively correlated with 5-DFS in lymph node–negative and –positive patients ($P < .05$), but RGB images were not in lymph node–positive patients ($P = .101$). Multivariate analysis indicated that the hazard ratio (HR) of HER2 MS was higher than that of HER2 RGB (HR = 2.454; 95% confidence interval [CI], 1.636-3.681 vs HR = 2.060; 95% CI, 1.361-3.119). Additionally, area under curve (AUC) by receiver operating characteristic analysis for HER2 MS was greater than that for HER2 RGB (AUC = 0.649; 95% CI, 0.577-0.722 vs AUC = 0.596; 95% CI, 0.522-0.670) in predicting the risk for recurrence. More importantly, the quantification of HER2 MS images has higher prediction accuracy than that of HER2 RGB images (69.6% vs 65.0%) on 5-DFS. Our study suggested that better information on BC prognosis could be obtained from the quantification of HER2 MS images and MS images might perform better in predicting BC prognosis than conventional RGB images.

Translational Oncology (2016) 9, 521–530

Introduction

Breast cancer (BC) is the most frequently diagnosed cancer and the leading cause of cancer death among females worldwide [1]. In China, the incidence of BC has been on a steady rise despite improvements in screening and comprehensive treatment [2]. Human epidermal growth factor receptor 2 (HER2), also known as c-erbB-2 or HER2/neu, is a commonly used theranostic biomarker for BCs, which is overexpressed in approximately 20% to 25% of invasive BCs [3–6]. Currently, the HER2-based molecular-targeted therapy plays a tremendous impact on BC prognosis [6–8]. Therefore, accurate quantitative determination of HER2 status is crucial for the establishment of BC treatment strategy in clinical practice.

Address all correspondence to: Yan Li, MD, PhD, Department of Oncology, Zhongnan Hospital of Wuhan University; Department of Peritoneal Cancer Surgery, Beijing Shijitan Hospital Affiliated to the Capital Medical University, No 10, Tieyi Road, Yangfangdian, Haidian District, Beijing, 100038, PR China.
E-mail: liyansd2@163.com

[1] This study was supported by the Key Project of the National Natural Science Foundation of China (no. 81230031/H18), the National Science Foundation of China (no. 62172274), and the Program for New Century Excellent Talents in Universities (no. NCET-10-0644).
Received 25 July 2016; Accepted 21 September 2016

1936-5233/16
http://dx.doi.org/10.1016/j.tranon.2016.09.007

Two methods are commonly reported for the assessment of HER2 status. One is immunohistochemistry (IHC) for the determination of HER2 protein expression, and the other is fluorescence *in situ* hybridization for the sensing of HER2 gene [9]. The former is recommended as a primary testing modality, and the latter is considered in ambiguous cause. However, interpreting IHC images by manual assessment is highly experience based and subjective. Additionally, no unified judgment and a lack of reproducibility as well as the potentially drastic variations among inter- and intraobservers further limited this technique [10,11]. Therefore, an accurate and repeatable quantitative method for IHC images becomes increasingly desirable in clinical histopathology. Computer image analysis of IHC images possessed the promising potential for more consistent interpretation and minimized the influence of subjective human factor compared with manual assessment [10,12]. However, the image quality would affect the analysis result no matter by pathologist or computer-aided image analysis [13]. Thus, it is a prerequisite to obtain high-quality IHC images and the related accurate quantitative analysis for the assessment of BC prognosis.

The conventional red-green-blue (RGB) imaging has been widely used, but their inherent technical limitations such as suboptimal image contrast and sharpness, overlapping chromogenic signals, and strong light effect affected the accuracy and repeatability of IHC image quantification and analysis obviously [14,15]. To address this issue, multispectral imaging (MSI) systems have been introduced and used for the separation of different cellular components and unmixing of overlapping chromogens [16,17]. Different from traditional RGB imaging, MSI can capture high-resolution images with a high degree of spectral information and facilitate the extraction of specific chromogen signal from the bright-field image even in the case of spatial and spectral overlap [17–19]. Moreover, the precise separation and independent quantitation of multiple markers in the subcellular compartments can be realized by MSI combined with advanced cell segmentation software [20].

In our previous study, the utility of MS images in quantitative IHC analysis showed higher sensitivity and accuracy, and better image quality and reliability than standard RGB images [15]. Furthermore, quantum dots–based MSI has been used for the obtainment of prognostic indicators of multiple proteins or genes in the tumor and tumor microenvironment [9,21,22]. But little is known concerning the prognostic value of quantitative assessment of bright-field MS images in BC patients. Herein, we employed MS and conventional RGB images for the quantitative analysis of HER2 IHC and compared the results to evaluate their performance in the prediction of BC prognosis.

Materials and Methods

Patients and Specimens

Complete tumor specimens from 240 invasive BC patients from our prospectively established BC database at our cancer center, which has been the source of our recent clinical studies on BC, were selected [9,23]. Major demographic and clinicopathologic characteristics were available, including age, tumor size, lymph node (LN) status, histological grade, hormone receptor status, and HER2 gene status. TNM staging and histological grade were classified according to the seventh edition of the American Joint Committee on Cancer TNM system [24] and the fourth edition of the WHO histological grade [25]. Major treatment information including types of surgery and adjuvant treatments (chemo/radiotherapy and endocrine therapy) was obtained from the medical records of each patient. The HER2-positive patients did not receive the molecular targeting therapy. All the patients were on regular follow-up schedule, and the complete information on 5-year disease-free survival (5-DFS) was available. Informed consents were obtained from all patients in the database, and the study was approved by the institutional review board and the ethics committee.

Tissue Microarray (TMA) Construction

All hematoxylin and eosin–stained slides were examined by independent reviewers who were blinded from the clinical features or outcomes. BC TMAs were constructed using standard procedures, as previously described [26]. Briefly, two cores were taken from each representative invasive tumor tissue (1.5 mm in diameter for each core). Then, 7 different TMAs sections with 240 tumor tissues were constructed (in collaboration with Shanghai Outdo Biotech Co. Ltd., Shanghai, China) (Figure 1*A1*).

Immunohistochemistry and Evaluation

Immunolocalization of HER2, estrogen receptor (ER), and progesterone receptor (PR) was performed using streptavidin-biotin peroxidase complex method. The IHC protocols were described previously [22]. In short (Figure 1*A2*), seven TMA sections were deparaffinized and dehydrated using a graded series of ethanol solutions. Endogenous peroxidase activity was blocked by 0.3% hydrogen peroxide for 10 minutes. Antigen retrieval was treated by microwave treatment in 0.01 M Tris-EDTA buffer (pH 9.0) for 20 minutes. Slides were incubated with primary antibodies of mouse antihuman polyclonal antibody against HER2 (A-0485, Dako, Denmark, dilution 1/50), rabbit anti-human monoclonal antibody against ER (sc-7207, Santa Cruz, USA, dilution 1/100), and PR (sc-7208, Santa Cruz, USA, dilution 1/100) for 2 hours at 37°C and then incubated with the corresponding horseradish peroxidase–conjugated secondary antibody (MaiXin Bio Co., Ltd., Fuzhou, China, 1:250 dilution) for 30 minutes at 37°C. Negative control was performed by omitting the primary antibody. Antigen-antibody reaction was visualized with 3,30′-diaminobenzidine (DAB) (DAKO, Denmark). After counterstaining with hematoxylin, sections were dehydrated through ascending alcohols.

The immunostaining results were determined independently by two expert pathologists (G.F.Y., J.P.Y.) without knowledge of patients' outcomes. The results of HER2 were scored from 0 to 3+ as the criteria described [6], and any discernable signals of ER and/or PR positive in the nucleus were defined as hormone receptor positive [27].

Image Acquisition, Quantification, and Analysis

The digital images of HER2 staining were captured based on 6 photographs for each core of TMAs under Olympus BX51 bright-field microscope equipped with Olympus DP72 RGB camera (Olympus Optical Co., Ltd., Tokyo, Japan) and CRi Nuance multispectral imaging systems (Cambridge Research & Instrumentation, Inc., Woburn, MA), respectively, at 100× magnification. The images of six photographs were integrated to form a panorama image for each TMAs core. The MS (Figure 1*B1*, *upper panel*) and RGB images (Figure 1*B3*, *upper panel*) of each core containing both tumor nests and stroma were acquired at the unified image acquisition parameters [15] by two imaging systems. A total of 6 spectral cubes from 420 to 720 nm in 20-nm increments were acquired by MSI

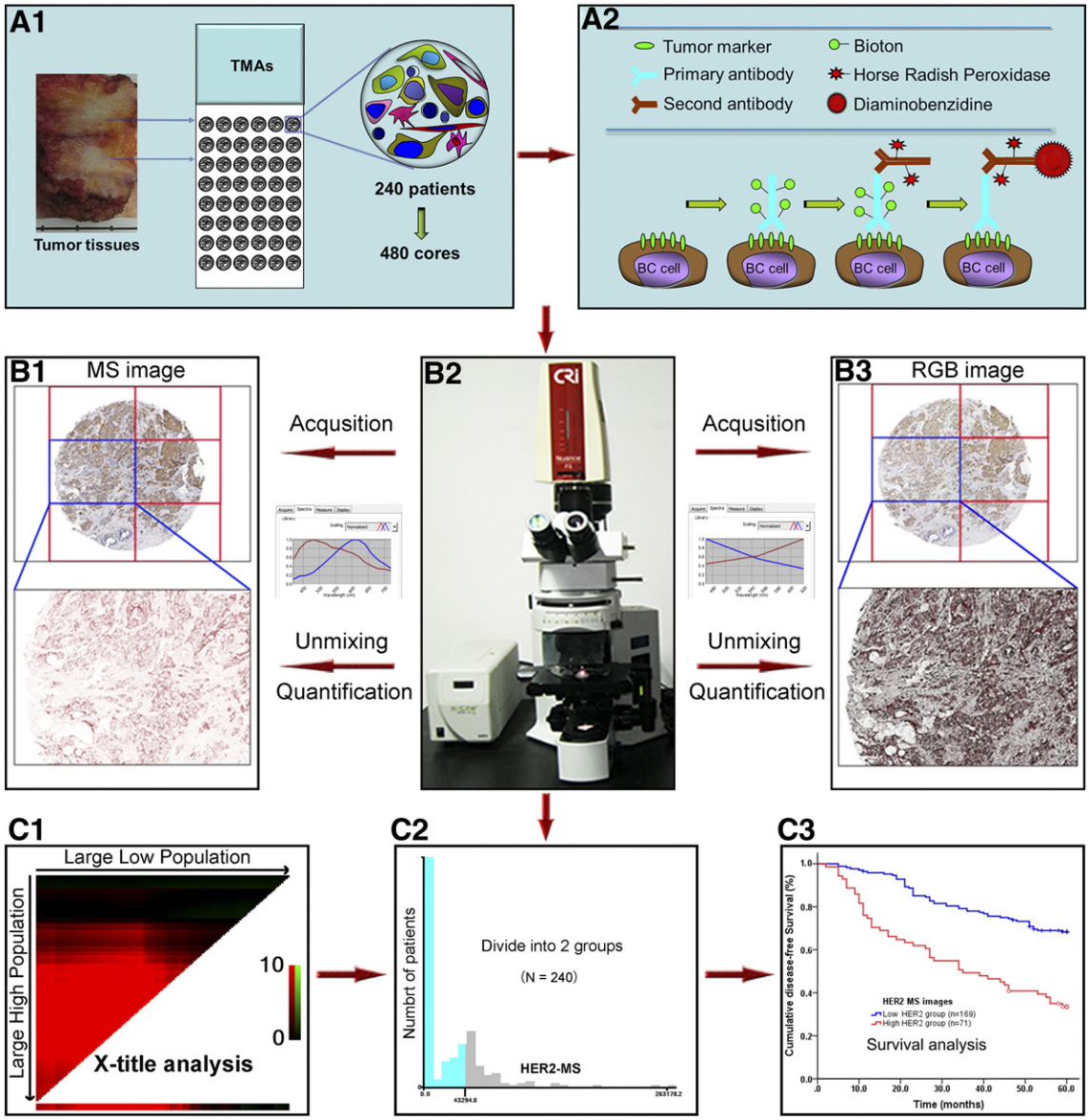

Figure 1. Flowchart of study design and major technical procedures. (A1) TMAs with 480 cores of 240 BC specimens were constructed. (A2) Three key molecule biomarkers of BC were stained by routine IHC method, staining HER2 in cell membrane. (B1–B3) The HER2 MS and RGB images were captured by MSI system, and their unmixing and quantification were obtained by CRi Nuance software. (C1–C3) HER2 MS and RGB image analysis outputs were analyzed by X-tile software (C1). All patients were divided into two groups (C2) and analyzed by Kaplan-Meier method (C3).

system. Finally, 2880 bright-field IHC images of HER2 were obtained including identical 1440 RGB images and 1440 MS images, and all images were saved in Tagged Image File Format with consistent resolution for further analysis.

After imaging acquisition, CRi Nuance software V 3.0.0 within MSI system was used for the unmixing and quantification in HER2 MS and RGB images with standard processing. The spectral characteristics (curve) for two chromogens (DAB and hematoxylin) in MS and RGB images were obtained by spectral separation. Detailed steps were previously described [15,28]. The target images with different spectra were automatically unmixed into DAB (Figure 1, *B1* and *B3*, *lower panel*) and hematoxylin (*data not shown*) component images by Nuance software based on spectral library. Nonspecific background signals were subtracted from each image individually. DAB spectral signals of HER2 were automatically quantified.

The original results produced by CRi Nuance software were total signal optical density (OD) values for HER2 in one view field. As each TMA core has six view fields, the final quantitative results output was HER2 sum, i.e., signal pixels in six fields altogether. To minimize errors in data interpretation and scoring as well as to improve data quality, average OD values of all the positive staining of HER2 in each image were measured. Once the HER2 total signal OD and average signal OD values in MS and RGB images were calculated, the X-tile software, which was explored and used to identify optimal cut point of biomarkers based on the prognosis by scholars at Yale University in 2004 [29], was applied to automatically identify the cutoff points of total OD and average OD values in HER2 MS and

RGB images, and all patients were categorized into two groups according their values (Figure 1, *C1–C3*).

Statistical Analysis

Statistical analyses were performed with SPSS 19.0 software (SPSS Institute, Chicago, IL). All numeric values are reported as the mean ± standard deviation. Correlation test was calculated by Pearson chi-square. The primary end point, 5-DFS, was calculated by the Kaplan-Meier method and analyzed by the log-rank test. Multivariate analysis was performed by the Cox proportional hazards model. Sensitivity, specificity, positive predictive values (PPVs), and negative predictive values (NPVs) were calculated. Receiver operating characteristic (ROC) curve analysis was used to determine the predictive value of the independent prognosis factors. Two-sided $P < .05$ was considered as statistically significant.

Results

IHC Staining Results in TMAs

The main clinicopathologic characteristics of 240 patients in BC TMAs were presented in Table 1. The median age of patients was 49.5 years (range, 21-89 years), and the average follow-up time was 45.6 months. IHC staining was performed in seven BC TMAs, and the result of each specimen was obtained for images-based digital analysis (Figure 2, *A–C*). HER2 protein was expressed in cell membrane of tumor cells. Among the 240 patients in this study, 162 (67.4%) cases were scored as 0/1+ HER2, 27 (11.3%) cases were scored as 2+, and 51 (21.3%) cases were scored as 3+ using the visual method. The corresponding MS and RGB images of HER2 were acquired, and some representative IHC images were shown in Figure 2, *D–I*. Consistent with our previous report [15], HER2 MS images presented better image qualities compared with RGB images for further computer analysis.

Table 1. Major Clinicopathologic Characteristics of 240 Patients in BC TMAs

Variables	Patients (N = 240)	%
Age (years)		
≤50	149	62.1
>50	91	37.9
Tumor size (cm)		
T1 (T ≤ 2)	36	15.0
T2 (2 < T ≤ 5)	162	67.5
T3 (T > 5)	42	17.5
LNs status		
Positive	131	54.6
Negative	109	45.4
Histological grade		
I	40	16.7
II	141	58.8
III	59	24.6
Clinical stage		
I, II	164	68.3
III, IV	76	31.7
Hormone receptor status *		
Positive	186	77.5
Negative	54	22.5
HER2 expression		
IHC 3+	51	21.3
IHC 2+	27	11.3
IHC 0-1+	162	67.4
HER2 gene status †		
Amplification	51	21.3
Nonamplification	189	78.7
Chemotherapy		
Yes	199	82.9
No	41	17.1
Radiotherapy		
Yes	47	19.6
No	193	80.4
Recurrence		
Yes	100	41.7
No	140	58.3

* ER and/or PR positive was defined as hormone receptor positive, which was determined by immunohistochemical staining according to guideline [27].

† HER2 gene was determined by fluorescent *in situ* hybridization according to guideline [6].

Quantification of MS Images and RGB Images of HER2 Expression for 5-DFS Prediction

Among the 240 specimens, the HER2 total signal OD values and the average signal OD values quantified by MS images (i.e., HER2 MS) varied from 0.00 to 2.63×10^5 (median, 1.60×10^4) and from 0.000 to 0.156 (median, 0.013), respectively. Determined by RGB images (i.e., HER2 RGB), the values were from 0.00 to 2.23×10^5 (median, 1.14×10^4) and from 0.000 to 0.138 (median, 0.009) accordingly (Tables 2 and 3). The cutoff value of the total signal OD values in HER2 MS identified by the X-tile software was 4.33×10^4, and based on this, patients were categorized into high–HER2 expression group (n = 71) and low–HER2 expression group (n = 169). The 5-DFS of the former was significant shorter than that of the latter (log-rank test, $P < .001$; Figure 3*A*). The cutoff point in HER2 RGB was 3.89×10^4, and patients with high HER2 expression (n = 62) had significantly worse 5-DFS than those with low HER2 expression (n = 178) by determining RGB images ($P < .001$) (Figure 3*B*).

Similarly, based on the judgment of X-tile software, the cutoff point of the average signal OD values in HER2 MS was 0.031, and patients were categorized into high-HER2 group (n = 73) and low-HER2 group (n = 167); the cutoff point of HER2 RGB was 0.026, and patients were divided into high-HER2 group (n = 65) and low-HER2 group (n = 175). Patients with high HER2 expression had significantly lower 5-DFS than those with low HER2 expression ($P < .001$), whether determined by HER2 MS (Figure 4*A*) or RGB images (Figure 4*B*).

The Quantification of HER2 MS Images and RGB Images to Predict 5-DFS by LN Status

We next evaluated the prediction of HER2 MS and RGB images in patients coupling with different LN status. As shown in Figure 3, by the determination of total signal OD index, HER2 expression evaluated by HER2 MS images was inversely correlated with 5-DFS in LN-positive patients ($P < .001$, Figure 3*C*) and LN-negative patients ($P = .007$, Figure 3*E*). For the quantification of HER2 RGB images, HER2 expression was negatively correlated with 5-DFS in LN-positive patients ($P < .001$, Figure 3*D*) but not in LN-negative patients ($P = .101$, Figure 3*F*). Similar results were also observed in the average signal OD index (Figure 4, *C–F*). These findings indicated that the quantitation of HER2 MS images might be a more preferable approach in predicting the 5-DFS in BC patients.

Multivariate and Weighted Analysis

To further explore the potential value of HER2 MS images for the predication of BC prognosis, a multivariate analysis was performed. The results demonstrated that, by the analysis of the total signal OD index from HER2 MS images, multivariate analysis could identify four variables—HER2 status ($P < .001$), LN status ($P = .006$), histological grade ($P < .001$), and clinical stage ($P = .048$)—as independent prognostic factors for 5-DFS. However, only three

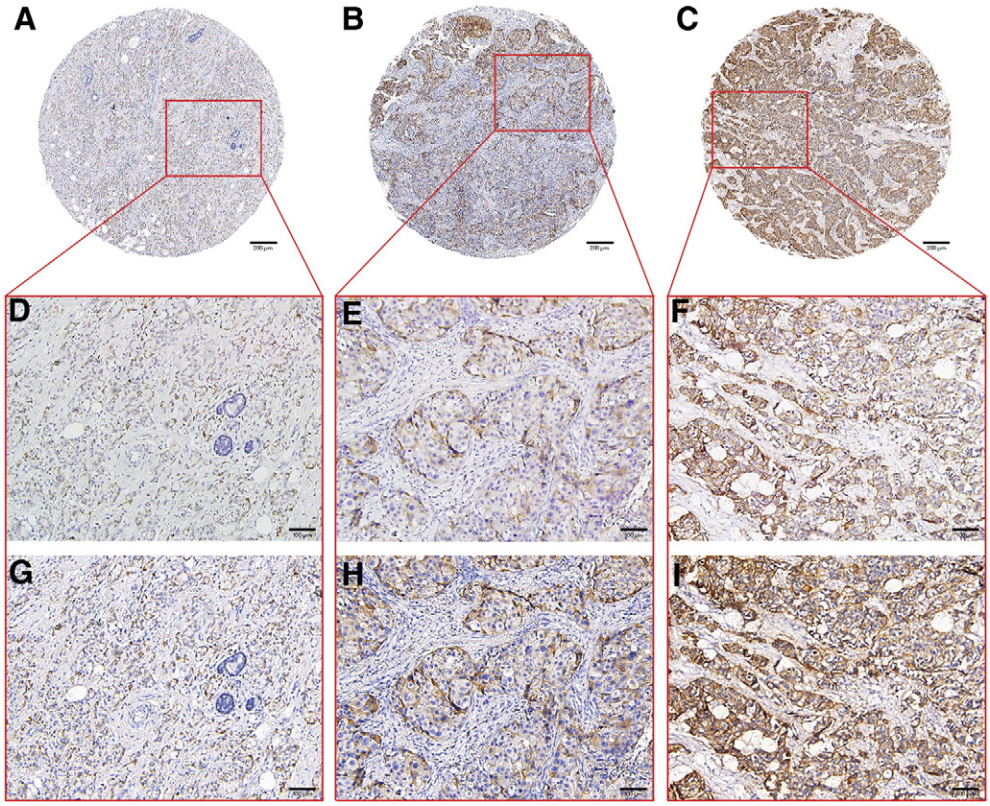

Figure 2. Immunohistological findings in BC TMAs. (A–C) Representative examples of HER2 scored as 1+, 2+, and 3+. (D–F) The RGB images were acquired by traditional RGB imaging system. (G–I) The corresponding MS images were acquired by MSI system. (D and G) Positive HER2 membrane staining was scored as 1+. (E and H) Positive HER2 membrane staining was scored as 2+. (F and I) Positive HER2 membrane staining was scored as 3+. Magnification 40× (A, B, and C) or 100× (D, E, F, G, H, and I); scale bar: 100 μm for all images.

variables including HER2 status (P = .001), LN status (P = .018), and histological grade (P < .001) could be identified from HER2 RGB images (Table 4). Similar results were also achieved by the determination of the average signal OD index (Table 5).

Additionally, the weighted analysis of the impacts of HER2 expressions quantified from HER2 MS images and RGB images on 5-DFS was carried out. As shown in Tables 4 and 5, the hazard ratios (HRs) of HER2 MS were higher than those of HER2 RGB (HR = 2.454; 95% CI, 1.636-3.681 vs HR = 2.060; 95% CI, 1.361-3.119; HR = 2.467; 95% CI, 1.650-3.688 vs HR = 2.401; 95% CI, 1.599-3.605) by either total signal OD index or average signal OD index.

Evaluation of the Prognostic Value of HER2 MS and HER2 RGB Images

ROC curve analysis was implemented to further evaluate the prognostic performance of these independent factors identified by multivariate analysis. All factors could predict the recurrence risk well (P < .05). In predicting recurrence or not, by the comparison of the total signal OD index, the prognostic value of HER2 MS images (AUC = 0.649; 95% CI, 0.577-0.722; P < .001) was higher than HER2 RGB images (AUC = 0.596; 95% CI, 0.522-0.670; P = .012) and clinical stage (AUC = 0.642; 95% CI, 0.571-0.713; P < .001) but lower than LN status (AUC = 0.696, 95% CI: 0.628-0.763, P < .001) and histological grade (AUC = 0.748, 95% CI: 0.686-0.811, P < .001) (Figure 5*A*). Analogous results were also revealed in the average signal OD index (Figure 5*B*).

Evaluation of Prediction Efficiency of HER2 MS and HER2 RGB Images

In addition, the prediction efficiency of HER2 MS and RGB images in prognostication of BC recurrence was also assessed. As shown in Table 6, by the comparison of the total signal OD index, sensitivity, specificity, PPV, and NPV of the prediction of BC prognosis by HER2 MS images were higher than those of HER2 RGB images (48.0% vs 39.0%, 84.2% vs 83.6%, 69.0% vs 62.9%,

Table 2. The Total Signal OD Index of HER2 MS and RGB Images, Cutoff Value, and Classification

Images	Total Signal OD Values		Cutoff Value	Patients (*n*)	
	Median	Range		High-HER2 Group	Low-HER2 Group
HER2 MS	1.60×10^4	$0.00\text{-}2.63 \times 10^5$	4.33×10^4	71	169
HER2 RGB	1.14×10^4	$0.00\text{-}2.23 \times 10^5$	3.89×10^4	62	178

Table 3. The Average Signal OD Index of HER2 MS and RGB Images, Cutoff Value, and Classification

Images	Average Signal OD Values		Cutoff Point	Patients (*n*)	
	Median	Range		High-HER2 Group	Low-HER2 Group
HER2 MS	0.013	0.000-0.156	0.031	73	167
HER2 RGB	0.009	0.000-0.138	0.026	65	175

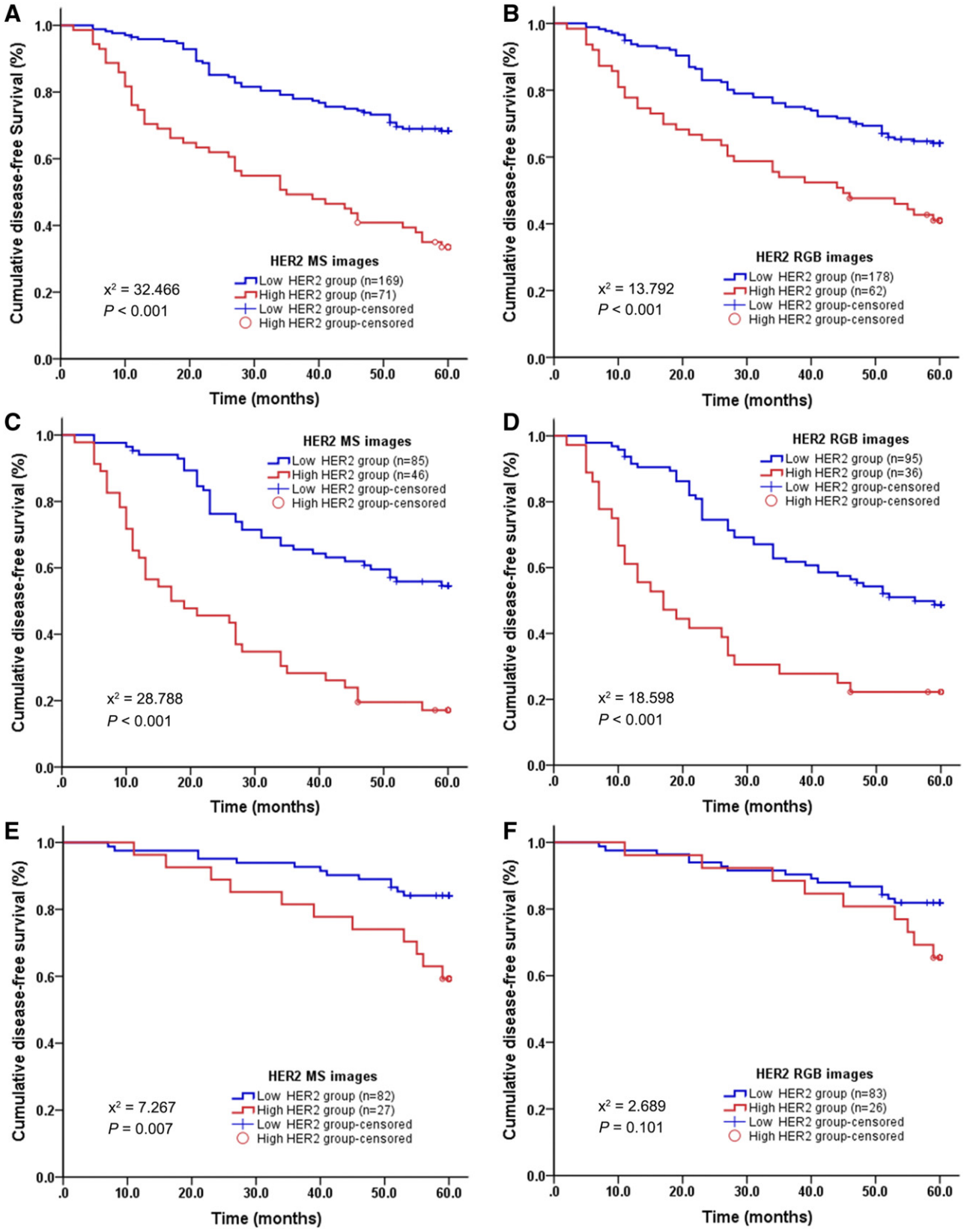

Figure 3. The relationship between total signal OD index and 5-DFS in BC patients, which was obtained from the analysis of HER2 MS or HER2 RGB images. HER2 MS (A) and HER2 RGB (B) are negatively related with 5-DFS in all patients. HER2 MS (C) and HER2 RGB (D) are inversely related with 5-DFS in LN-positive patients. HER2 MS (E) is negatively related with 5-DFS in LN-negative patients, but HER2 RGB (F) has no statistical significance in LN-negative patients. *P* value tested by the log-rank test.

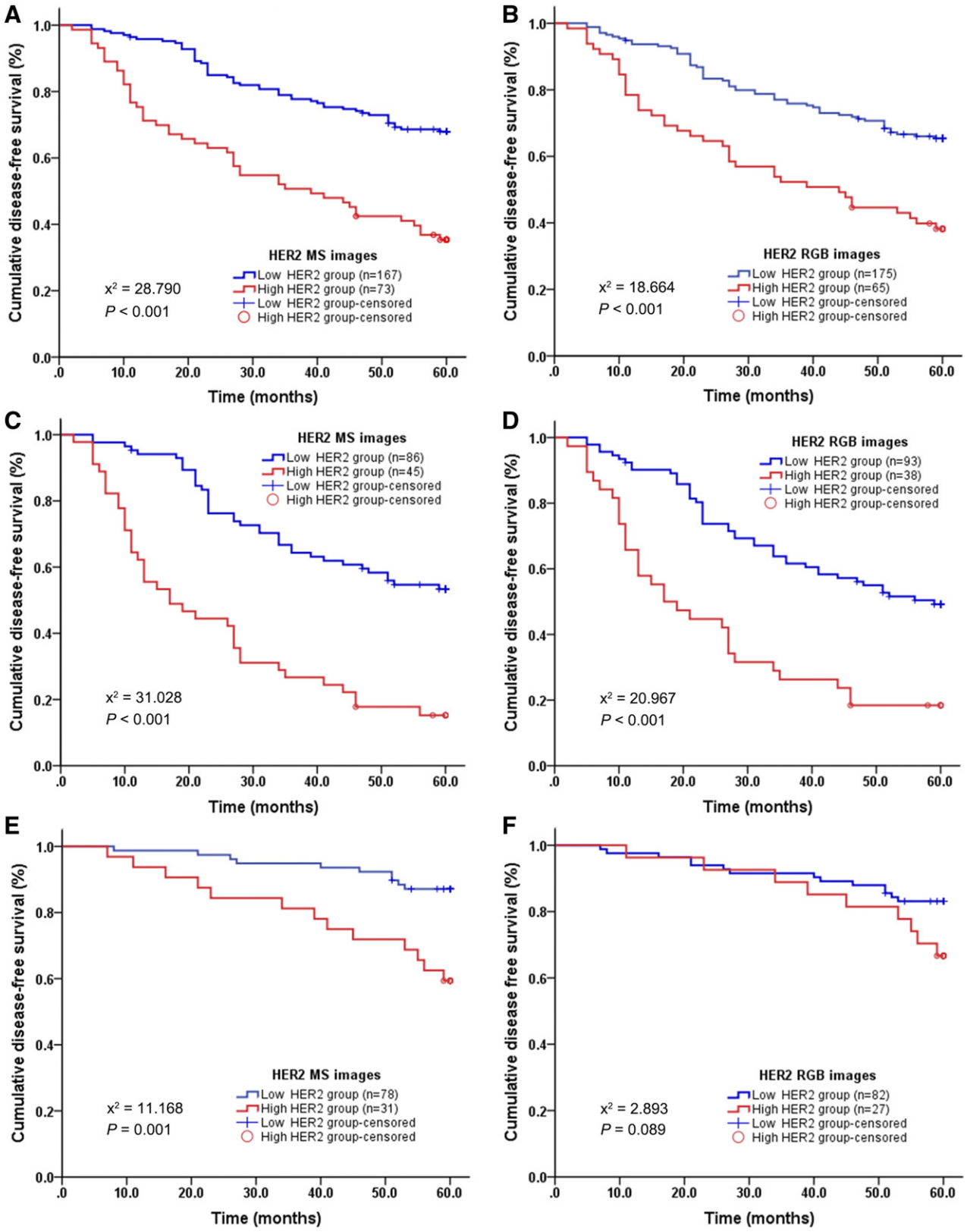

Figure 4. The relationship between average signal OD index and 5-DFS in BC patients, which was obtained from the analysis of HER2 MS or HER2 RGB images. (A–F) Similar results were further observed. *P* value tested by the log-rank test.

and 69.8% vs 65.7%, respectively). The higher predictive accuracy on recurrence was thus obtained for HER2 MS images than HER2 RGB images (69.6% vs 65.0%). The same trend was also observed by the determination of the average signal OD index (69.6% vs 64.6%).

Discussion

In the present study, we have developed a novel approach to quantitatively determine the HER2 expression in IHC images automatically for the better evaluation of the prognosis of BC

Table 4. Multivariate analyses of factors associated with 5-DFS by total signal OD index.

Factors	Analysis from HER2 MS images		Analysis from HER2 RGB images	
	HR (95% CI)	*P* Value	HR (95% CI)	*P* Value
Tumor size	1.131 (0.753-1.698)	.552	1.178 (0.789-1.758)	.422
LN status	2.260 (1.257-3.061)	**.006**	2.029 (1.129-3.645)	**.018**
Hormone receptor status	0.760 (0.491-1.174)	.216	0.706 (0.458-1.089)	.115
HER2 status	2.454 (1.636-3.681)	< **.001**	2.060 (1.361-3.119)	**.001**
Histological grade	2.924 (2.000-4.275)	< **.001**	2.143 (2.156-4.580)	< **.001**
Clinical stage	1.572 (1.005-2.460)	**.048**	1.451 (0.926-2.275)	.105

5-DFS, 5-year disease-free survival; HR, HR; CI, confidence interval; HER2, human epidermal growth factor receptor-2; LN, LN; OD, OD.

patients. The quantitation of MS images or conventional RGB images of HER2 IHC was realized by the use of TMAs of large cohorts of BC tissue samples. To the best of our knowledge, it is the first time to quantify the HER2 status by MS images and display their closer relationship with the recurrence-free survival in BC patients. Additionally, such quantification by MS images performed better in predicting BC prognosis than that by RGB images. Coupled with our previous research about the behavior of MSI in IHC analysis [15], it showed that MSI has the potential as a standard digital imaging system for both diagnosis and prediction of BC prognosis in clinical pathology.

With the development of precision medicine, quantitative pathology with improved imaging technique and image information acquisition and analysis has attracted more and more attention. In the aspect of imaging technique, MSI can obtain color spectrum information at every pixel of a color image rather than specific color information of the three available channels (red, green, and blue) by standard RGB imaging [14,30]. MSI collects different spectral images (from 420 to 720 nm, covering most chromogens) with accurate spectral content, and a complete image "stack" is assembled in memory where a spectrum is correlated with every pixel. This ability significantly improves the efficiency and accuracy of imaging process, providing a promising way for multiple target imaging under both bright-field and fluorescence view [17–19,30]. In this study, we employed RGB imaging and MSI system to get HER2 IHC staining images in BC TMAs and compared their behaviors. Similar with the result reported by Boucheron et al. [31], MS images provided better overall image qualities and more useful information than the standard RGB images which were vital for further computer analysis.

In the aspect of image information acquisition and analysis, the CRi Nuance MSI system can allow pathologists to precisely separate and quantify multiple spatially colocalized chromogens in multicolor IHC staining by multispectral linear unmixing. It can also realize an accurate segmentation of different tissue morphologies (e.g., tumor versus stroma) and cellular and subcellular compartments [17,32–35]. In our previous study, better segmentation accuracy and richer color information have been obtained from unmixing MS images of IHC staining combined MSI with CRi Nuance software [15]. Xu et al. also reported the potential utility of CRi Nuance MSI system in quantifying biomarkers and interpreting the spatial and anatomical distribution of biomarkers of high-order processes [36].

Table 5. Multivariate analyses of factors associated with 5-DFS by average signal OD index.

Factors	Analysis from HER2 MS images		Analysis from HER2 RGB images	
	HR (95% CI)	*P* Value	HR (95% CI)	*P* Value
Tumor size	1.150 (0.769-1.722)	.496	1.202 (0.809-1.786)	.362
LN status	2.086 (1.162-3.743)	**.014**	2.243 (1.251-4.023)	**.007**
Hormone receptor status	0.814 (0.520-1.275)	.369	0.811 (0.515-1.277)	.365
HER2 status	2.467 (1.650-3.688)	< **.001**	2.401(1.599-3.605)	< **.001**
Histological grade	3.017 (2.065-4.408)	< **.001**	3.293 (2.259-4.801)	< **.001**
Clinical stage	1.585 (1.013-2.480)	**.044**	1.472 (0.940-2.306)	.091

5-DFS, 5-year disease-free survival; HR, HR; CI, confidence interval; HER2, human epidermal growth factor receptor-2; LN, LN; OD, OD.

HER2 status, which is closely related to the malignant biologic behaviors of BC, including aggressiveness and metastasis, has been used as a critical indicator for the identification of distinct biological subtypes of BC and prediction of prognosis [9,37]. Quantum dots–based quantitative spectral analysis of HER2 has helped the establishment of a new molecular classification system of BC and the prediction of tumor prognosis [23]. MSI has been reported to detect some potential prognostic factors [36] and to determine the pericyte coverage of differentiated vessels inside tumor vasculature as an independent unfavorable prognostic factor for patients with clear cell renal cell carcinoma [38,39].

Based on this new approach, the present study systematically evaluated the clinical value of the quantitation of HER2 MS images and RGB images coupled with the conventional pathological prognostic factors using 5-DFS as the primary end point. All BC patients were divided into two subgroups with different 5-DFS according to X-title software. The result showed that more patients in the poor-prognosis group were identified by quantifying HER2 MS images than those by quantifying RGB images, which were both inversely correlated with 5-DFS significantly. We further assessed the prognostic value of HER2 MS and RGB images by LN status, the most important indicator for evaluating tumor metastasis. Significant correlation between HER2 RGB and 5-DFS only existed in LN-positive patients, not in LN-negative patients. Nevertheless, HER2 MS exhibited statistical significance in both LN-positive and LN-negative patients (Figures 3 and 4), suggesting the better predictive ability of HER2 MS on recurrence than HER2 RGB.

Multivariate analysis indicated that HER2 MS provided higher HR than HER2 RGB in predicting 5-DFS (2.454 vs 2.060; 2.467 vs 2.401). Furthermore, HER2 MS had correlation with three major conventional prognostic factors, including LN status, histological grade, and clinical stage, but HER2 RGB was only correlated with the first two factors (Tables 4 and 5). Additionally, ROC curve analysis showed that HER2 MS had higher prognostic value on recurrence than HER2 RGB (Figure 5, *A* and *B*). Compared with HER2 RGB, HER2 MS displayed better performance in sensitivity, accuracy, PPV, and NPV for predicting recurrences (Table 6). Thus, the quantification of HER2 MS images could be used as a better approach for prognostic prediction, benefitting from the better predictive ability among BC subgroups, better performance for recurrence prediction, and good correlation with the currently established pathological prognosticators.

We acknowledge some limitations to our study. Firstly, the results should be evaluated further in a larger multicenter BC patient population with long-term follow-up. Secondly, only the relationship between HER2 expression and patient outcome by 5-DFS was evaluated in this study. It is better to further study the corresponding relations between HER2 expression and the overall survival because of the nonlinear relation between DFS and overall survival sometimes. Thirdly, although image analysis techniques can reduce interobserver

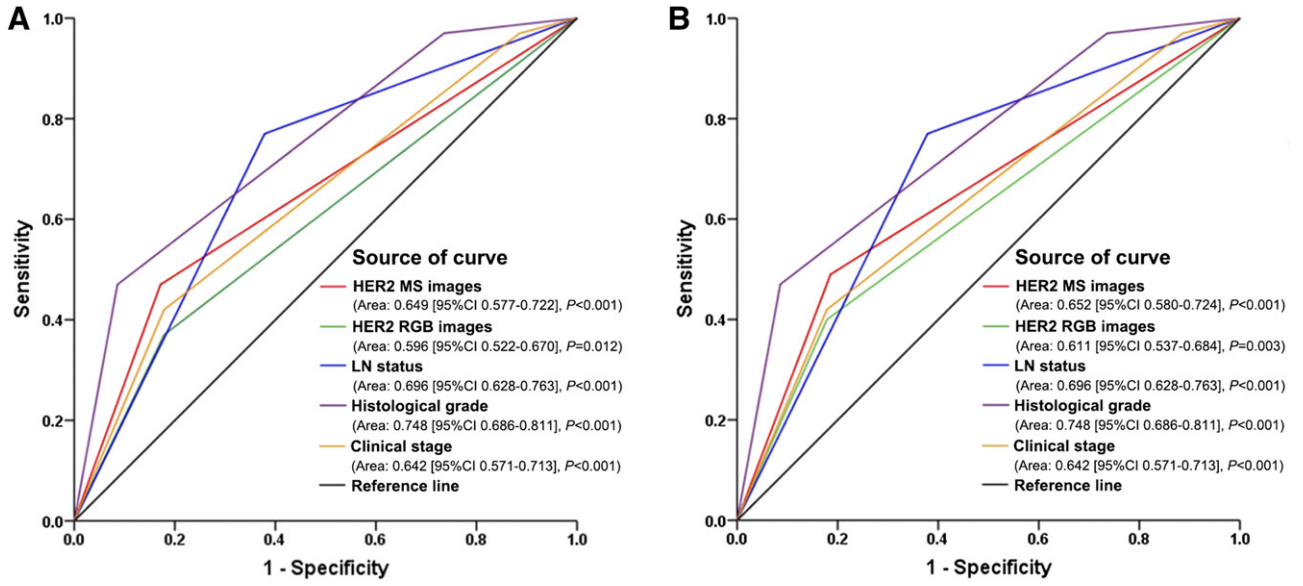

Figure 5. ROC curve analysis on the prognostic value of HER2 MS and HER2 RGB. (A) By the analysis of total signal OD index, AUC of HER2 MS was greater than HER2 RGB and clinical stage but smaller than LN status and histological grade on recurrence. (B) Similar results were further realized by the determination of average signal OD index.

variability, it is impossible to eliminate all subjectivities because the system was trained manually by a pathologist initially. Finally, the limitation that every core of TMAs was not able to completely represent the whole tumor might lead to the possible sample selection bias.

Conclusions

In this study, we developed an approach for the assessment of HER2 status using quantifying MS images and validated the potential of MS images on predicting outcome in patients with invasive BC. Our findings demonstrated that better information on BC prognosis could be obtained from the quantification of HER2 MS images and the application of MS images may be better than conventional RGB images in predicting BC prognosis.

Conflicts of Interest

None.

Acknowledgement

This study was supported by the Key Project of the National Natural Science Foundation of China (no. 81230031/H18), the National Science Foundation of China (no. 62172274), and Program for New Century Excellent Talents in Universities (no. NCET-10-0644).

Table 6. The prediction efficiency of HER2 MS and HER2 RGB images for BC prognosis.

Items	Analysis from total signal OD index		Analysis from average signal OD index	
	HER2 MS images	HER2 RGB images	HER2 MS images	HER2 RGB images
Sensitivity (%)	48.0 (49/100)	39.0 (39/100)	51.0 (51/100)	40.0 (40/100)
Specificity (%)	84.2 (118/140)	83.6 (117/140)	82.9 (116/140)	82.1 (115/140)
PPV (%)	69.0 (49/71)	62.9 (39/62)	68.0 (51/75)	61.5 (40/65)
NPV (%)	69.8 (118/169)	65.7 (117/178)	70.3 (116/165)	65.7 (115/175)
Accuracy (%)	69.6 (167/240)	65.0 (156/240)	69.6 (167/240)	64.6 (155/240)

BC, BC; HER2, human epidermal growth factor receptor-2; OD, OD; PPV, positive predictive value; NPV, negative predictive value.

References

[1] Torre LA, Bray F, Siegel RL, Ferlay J, Lortet-Tieulent J, and Jemal A (2015). Global cancer statistics, 2012. *CA Cancer J Clin* **65**(2), 87–108.

[2] Miao H, Hartman M, Bhoo-Pathy N, Lee SC, Taib NA, Tan EY, Chan P, Moons KG, Wong HS, and Goh J, et al (2014). Predicting survival of de novo metastatic breast cancer in Asian women: systematic review and validation study. *PLoS One* **9**(4), e93755.

[3] Benson JR, Jatoi I, Keisch M, Esteva FJ, Makris A, and Jordan VC (2009). Early breast cancer. *Lancet* **373**(9673), 1463–1479.

[4] Freudenberg JA, Wang Q, Katsumata M, Drebin J, Nagatomo I, and Greene MI (2009). The role of HER2 in early breast cancer metastasis and the origins of resistance to HER2-targeted therapies. *Exp Mol Pathol* **87**(1), 1–11.

[5] Moasser MM (2007). The oncogene HER2: its signaling and transforming functions and its role in human cancer pathogenesis. *Oncogene* **26**(45), 6469–6487.

[6] Wolff AC, Hammond ME, Hicks DG, Dowsett M, McShane LM, Allison KH, Allred DC, Bartlett JM, Bilous M, and Fitzgibbons P, et al (2013). Recommendations for human epidermal growth factor receptor 2 testing in breast cancer: American Society of Clinical Oncology/College of American Pathologists clinical practice guideline update. *J Clin Oncol* **31**(31), 3997–4013.

[7] Hudis CA (2007). Trastuzumab—mechanism of action and use in clinical practice. *N Engl J Med* **357**(1), 39–51.

[8] Liberato NL, Marchetti M, and Barosi G (2007). Cost effectiveness of adjuvant trastuzumab in human epidermal growth factor receptor 2–positive breast cancer. *J Clin Oncol* **25**(6), 625–633.

[9] Chen C, Xia HS, Gong YP, Peng J, Peng CW, MB H, Zhu XB, Pang DW, Sun SR, and Li Y (2010). The quantitative detection of total HER2 load by quantum dots and the identification of a new subtype of breast cancer with different 5-year prognosis. *Biomaterials* **31**(33), 8818–8825.

[10] Mohammed ZM, Going JJ, McMillan DC, Orange C, Mallon E, Doughty JC, and Edwards J (2012). Comparison of visual and automated assessment of HER2 status and their impact on outcome in primary operable invasive ductal breast cancer. *Histopathology* **61**(4), 675–684.

[11] Di Cataldo S, Ficarra E, and Macii E (2012). Computer-aided techniques for chromogenic immunohistochemistry: status and directions. *Comput Biol Med* **42**(10), 1012–1025.

[12] Byrne A and Hilbert DR (2003). Color realism and color science. *Behav Brain Sci* **26**(1), 3–21 [22-63].

[13] Tani S, Fukunaga Y, Shimizu S, Fukunishi M, Ishii K, and Tamiya K (2012). Color standardization method and system for whole slide imaging based on spectral sensing. *Anal Cell Pathol (Amst)* **35**(2), 107–115.

[14] Stack EC, Wang C, Roman KA, and Hoyt CC (2014). Multiplexed immunohistochemistry, imaging, and quantitation: a review, with an assessment of tyramide signal amplification, multispectral imaging and multiplex analysis. *Methods* **70**(1), 46–58.

[15] Liu WL, Wang LW, Chen JM, Yuan JP, Xiang QM, Yang GF, AP Q, Liu J, and Li Y (2016). Application of multispectral imaging in quantitative immunohistochemistry study of breast cancer: a comparative study. *Tumour Biol* **37**(4), 5013–5024.

[16] Mansfield JR (2010). Cellular context in epigenetics: quantitative multicolor imaging and automated per-cell analysis of miRNAs and their putative targets. *Methods* **52**(4), 271–280.

[17] Blenman KR and Lee PP (2014). Quantitative and spatial image analysis of tumor and draining lymph nodes using immunohistochemistry and high-resolution multispectral imaging to predict metastasis. *Methods Mol Biol* **1102**, 601–621.

[18] Levenson RM and Mansfield JR (2006). Multispectral imaging in biology and medicine: slices of life. *Cytometry A* **69**(8), 748–758.

[19] Themelis G, Yoo JS, and Ntziachristos V (2008). Multispectral imaging using multiple-bandpass filters. *Opt Lett* **33**(9), 1023–1025.

[20] Levenson RM, Fornari A, and Loda M (2008). Multispectral imaging and pathology: seeing and doing more. *Expert Opin Med Diagn* **2**(9), 1067–1081.

[21] Yuan JP, Wang LW, AP Q, Chen JM, Xiang QM, Chen C, Sun SR, Pang DW, Liu J, and Li Y (2015). Quantum dots–based quantitative and in situ multiple imaging on ki67 and cytokeratin to improve ki67 assessment in breast cancer. *PLoS One* **10**(4), e0122734.

[22] Peng CW, Liu XL, Liu X, and Li Y (2010). Co-evolution of cancer microenvironment reveals distinctive patterns of gastric cancer invasion: laboratory evidence and clinical significance. *J Transl Med* **8**, 101.

[23] Chen C, Sun SR, Gong YP, Qi CB, Peng CW, Yang XQ, Liu SP, Peng J, Zhu S, and MD H, et al (2011). Quantum dots–based molecular classification of breast cancer by quantitative spectroanalysis of hormone receptors and HER2. *Biomaterials* **32**(30), 7592–7599.

[24] Edge SB, Byrd DR, Compton CC, Fritz AG, Greene FL, and Trotti A (2010). AJCC Cancer Staging Manual. . 7th ed.New York: Springer; 2010 .

[25] Lakhani SR, Ellis IO, Schnitt SJ, Tan PH, and van de Vijver MJ (2012). WHO classification of tumours of the breast. World Health Organization Classification of Tumours. 4th ed. Lyon: IARC Press; 2012.

[26] Zhu XD, Zhang JB, Zhuang PY, Zhu HG, Zhang W, Xiong YQ, WZ W, Wang L, Tang ZY, and Sun HC (2008). High expression of macrophage colony-stimulating factor in peritumoral liver tissue is associated with poor survival after curative resection of hepatocellular carcinoma. *J Clin Oncol* **26**(16), 2707–2716.

[27] Hammond ME, Hayes DF, Dowsett M, Allred DC, Hagerty KL, Badve S, Fitzgibbons PL, Francis G, Goldstein NS, and Hayes M, et al (2010). American Society of Clinical Oncology/College of American Pathologists guideline recommendations for immunohistochemical testing of estrogen and progesterone receptors in breast cancer. *J Clin Oncol* **28**(16), 2784–2795.

[28] 30Nuance™ 3.0 Quick Start Guide. P/N 130805 Rev. 00. Caliper Life Sciences, Inc., 68 Elm St., Hopkinton, MA, 01748, USA 508-435-9500. www.CaliperLS.com.

[29] Camp RL, Dolled-Filhart M, and Rimm DL (2004). X-tile: a new bio-informatics tool for biomarker assessment and outcome-based cut-point optimization. *Clin Cancer Res* **10**(21), 7252–7259.

[30] Irshad H, Gouaillard A, Roux L, and Racoceanu D (2014). Multispectral band selection and spatial characterization: application to mitosis detection in breast cancer histopathology. *Comput Med Imaging Graph* **38**(5), 390–402.

[31] Boucheron LE, Bi Z, Harvey NR, Manjunath B, and Rimm DL (2007). Utility of multispectral imaging for nuclear classification of routine clinical histopathology imagery. *BMC Cell Biol* **8**(Suppl. 1), S8.

[32] Huang W, Hennrick K, and Drew S (2013). A colorful future of quantitative pathology: validation of Vectra technology using chromogenic multiplexed immunohistochemistry and prostate tissue microarrays. *Hum Pathol* **44**(1), 29–38.

[33] Levenson R, Beechem J, and McNamara G (2013). Spectral imaging in preclinical research and clinical pathology. *Stud Health Technol Inform* **185**, 43–75.

[34] Fiore C, Bailey D, Conlon N, Wu X, Martin N, Fiorentino M, Finn S, Fall K, Andersson SO, and Andren O, et al (2012). Utility of multispectral imaging in automated quantitative scoring of immunohistochemistry. *J Clin Pathol* **65**(6), 496–502.

[35] Wang LW, AP Q, Liu WL, Chen JM, Yuan JP, Wu H, Li Y, and Liu J (2016). Quantum dots–based double imaging combined with organic dye imaging to establish an automatic computerized method for cancer Ki67 measurement. *Sci Rep* **6**, 20564.

[36] Xu X, Gimotty PA, Guerry D, Karakousis G, Van Belle P, Liang H, Montone K, Pasha T, Ming ME, and Acs G, et al (2008). Lymphatic invasion revealed by multispectral imaging is common in primary melanomas and associates with prognosis. *Hum Pathol* **39**(6), 901–909.

[37] Xiang QM, Wang LW, Yuan JP, Chen JM, Yang F, and Li Y (2015). Quantum dot-based multispectral fluorescent imaging to quantitatively study co-expressions of Ki67 and HER2 in breast cancer. *Exp Mol Pathol* **99**(1), 133–138.

[38] Mansfield JR (2014). Multispectral imaging: a review of its technical aspects and applications in anatomic pathology. *Vet Pathol* **51**(1), 185–210.

[39] Cao Y, Zhang ZL, Zhou M, Elson P, Rini B, Aydin H, Feenstra K, Tan MH, Berghuis B, and Tabbey R, et al (2013). Pericyte coverage of differentiated vessels inside tumor vasculature is an independent unfavorable prognostic factor for patients with clear cell renal cell carcinoma. *Cancer* **119**(2), 313–324.